To: **Journal of The Electrochemical Society**

Microstructure, Proton Concentration and Proton Conductivity of Barium Zirconate Doped with Ho, Er, Tm and Yb

Donglin Han [a, *], Naoyuki Hatada [a], and Tetsuya Uda [a, *]

[a] Department of Materials Science and Engineering, Kyoto University,

Yoshida Honmachi, Sakyo-ku, Kyoto 606-8501, Japan

* Corresponding authors: Donglin Han (han.donglin.8n@kyoto-u.ac.jp)

and Tetsuya Uda (uda_lab@aqua.mtl.kyoto-u.ac.jp)

TEL: +81-75-753-5445, FAX: +81-75-753-5284

Abstract

Acceptor-doped $BaZrO_3$ is very attractive due to their high proton conductivity in wet atmosphere, enabling a promising application in electrochemical devices. In this work, a systematic investigation on $BaZrO_3$ doped with Ho, Er, Tm and Yb was performed. The results revealed that, a single perovskite phase was obtained when dopant with the content between 0.02 and 0.3 was introduced, regardless of whether Ho, Er, Tm or Yb was doped. And a bimodal microstructure was observed with the dopant content varying from 0.05 to 0.15. Such bimodal microstructure was found to be composed of large grains with homogeneous composition, and fine grains with discrepancy in composition. Then, through the study on electrochemical conductivity, when the dopant content was between 0.02 and 0.2, the samples doped with Tm was found to have the lowest activation energy for bulk conduction in wet H_2. Such result indicates that Tm possibly imparts $BaZrO_3$ with relatively low association energy for proton trapping. Furthermore, a comparison on the total conductivity suggested that $BaZr_{0.8}Ho_{0.2}O_{3-\delta}$, $BaZr_{0.8}Er_{0.2}O_{3-\delta}$, $BaZr_{0.8}Yb_{0.2}O_{3-\delta}$, $BaZr_{0.8}Tm_{0.2}O_{3-\delta}$ and $BaZr_{0.75}Tm_{0.25}O_{3-\delta}$ had comparably high value satisfying the criterion (> 0.01 Scm^{-1}) for the application as an electrolyte in fuel cells at 600 ^oC.

1. Introduction

Beginning from 1980th when proton conduction in solid oxides was discovered by Iwahara, *et al* [1, 2], materials with this special conduction property have being received increasing attention, due to their prospective applications in electrochemical devices [3-8]. Currently, the most promising candidate is acceptor-doped $BaZrO_3$, in which tetravalent Zr host cations are generally substituted by aliovalent dopants to produce oxide ion vacancies. Protons are thereby introduced through a hydration reaction with the participant of the oxide ion vacancies. [9]

Referring to the dopant candidate, Y is regarded as a good one [10-13], but research on finding the optimal dopant for $BaZrO_3$ has never stopped. Our recent work [12, 14] revealed that, besides Y, other rare earth elements of Ho, Er, Tm and Yb also imparted $BaZrO_3$ with high proton conductivity comparable with that of the Y-doped one. Such finding not only offers a flexible choice on the dopants, but also suggests the possibility to determine the optimal dopant for proton conductive $BaZrO_3$. But first of all, we believe that a detailed investigation on revealing the doping effect of Ho, Er, Tm and Yb on the properties of $BaZrO_3$ is needed. In this work, Ho, Er, Tm and Yb were doped into $BaZrO_3$ with various contents. Phase identification and microstructure observation were performed, together with the water content and proton conductivity measurements.

2. Experimental

2.1 Material preparation

Samples with the nominal composition of $BaZr_{1-x}M_xO_{3-\delta}$ (BZM, M = Ho, Er, Tm and Yb, x = 0.02, 0.05, 0.1, 0.15, 0.2, 0.25 and 0.3) were prepared by a conventional solid state reaction method. Starting materials of $BaCO_3$, ZrO_2, and Ho_2O_3, Er_2O_3 Tm_2O_3 or Yb_2O_3 were mixed at the desired ratios, and ball-milled (rotation speed about 300 rpm) for 24 h. Mixtures were then pressed into pellets under 9.8 MPa and heat-treated at 1000 ^oC for 10 h. After ball-milling for 10 h, the samples were pressed into pellets under 9.8 MPa again, and kept at 1300 ^oC for 10 h for synthesizing. The samples were ball-milled for 100 h, and subsequently mixed with a binder (NCB-166, DIC Corporation, Tokyo, Japan). The mixtures were then pressed into pellets at 392 MPa, and heat-treated at 600 ^oC for 8 h to remove the binder. At last, after being buried in sacrificial powders which are mixtures of the relevant synthesized BZM20 powders (99 wt%) and $BaCO_3$ (1 wt%), the pellet-like samples were heated at 1600 ^oC for 24 h in oxygen atmosphere for sintering.

2.2 Characterization

X-ray diffraction (XRD) measurements were performed on powder samples at room temperature using Cu *Kα* radiation with X'Pert-ProMPD (PANalytical, Almelo, Netherland). Rietveld refinement was carried out utilizing a commercial software X'Pert HighScore Plus to determine lattice constants. Microstructures were observed by scanning electron microscopy (SEM) and scanning transmission

electron microscopy (STEM) with VE-7800 (Keyence Co., Osaka, Japan) and JEM-2100F (JEOL, Tokyo, Japan), respectively. Samples for STEM observations were thinned by an argon ion (Ar^+) beam using a JEOL EM-09100IS Ion Slicer. The local composition was identified by STEM-EDS with JEOL JED-2300.

Karl-Fischer titration method was applied to determine water content. The pellet-like samples heat-treated at 1600 ^oC for sintering were broken into pieces about 2 mm in length, and hydrated in wet Ar with a water partial pressure of 0.05 atm for at least 6 days at 300 or 600 ^oC. Readers are referred to our previous works [15] for detailed procedures.

Conductivity measurements of the pellet-like samples with sputtered platinum (Pt) electrodes were performed in wet H_2 atmosphere. Pt plates wiped with silver mesh are used as current collector. Pt wire is used to lead the current to a frequency response analyzer (Solartron SI 1260, Solartron Analytical, Farnborough, UK). During the measurements, water partial pressure in the wet atmosphere was kept at 0.05 atm. The impedance spectra were collected in the frequency range from 10 Hz to 7 MHz with applied voltage of 100 mV at temperature from 600 to 100 ^oC.

3. Results

3.1 XRD Analysis

The as-sintered samples at 1600 ^oC with all the compositions prepared in this work were identified to be a single perovskite phase. Powder XRD patterns of the Tm-doped ones are shown in **Fig. 1(a)** for

example. A clear peak shift towards low angle side occurred (**Fig. 1(b)**), indicating a lattice expansion, with the increasing Tm content. Then, Rietveld refinement was performed on the XRD patterns using a cubic perovskite ($Pm\bar{3}m$) model [16, 17] to determine the lattice constant. As shown in **Fig. 2**, it is clear that the samples doped with Ho, Er, Tm and Yb increased with the increasing dopant content, because the six-coordinated radii of trivalent Ho (0.901 Å), Er (0.890 Å), Tm (0.880 Å) and Yb (0.868 Å) are larger than that of the tetravalent Zr cations (0.72 Å) [18].

3.2 Microstructure Observation

Fractured cross-section of the samples sintered at 1600 ^{o}C was subjected to SEM observation. Change in microstructure with the dopant content behaves in a similar way, regardless of whether Ho, Er, Tm or Yb is doped, with the case of the Tm-doped samples shown for example in **Fig. 3**. The grain of the undoped $BaZrO_3$, and the one doped with very small Tm content of 0.02 are relatively of uniform size. However, when the Tm content is increased to 0.05, 0.1 and 0.15, a bimodal microstructure formed with a clear co-existence of large grains and fine grains. Such phenomenon was also observed in a previous work of our group [12]. When the Tm content is further increased over 0.2, not only an improvement in the uniformity of grain size, but also a significant growth of grain size occurred. And compared with the sample containing the Tm content of 0.2, the grain size further increased when the Tm content was elevated to 0.25 and 0.3.

The microstructure of $BaZr_{0.85}Tm_{0.15}O_{3-\delta}$ was also observed by STEM, as shown in **Fig. 4**. A clear

coexistence of large grains and fine grains was confirmed, in agreement with that observed by SEM (**Fig. 3(d)**). Then, STEM-EDS point analysis with the spot size about 1 nm was applied to determine the local composition of the individual large grains and fine grains. An example of places for STEM-EDS point analysis on large grains (marked as L1 to L5) and fine grains (marked as F1 to F5) are shown in **Fig. 4**. With such method, several other different areas were examined, leading to the summarization in **Fig 5(a)** and **(b)** to give a statistical evaluation on the compositions of the large and fine grains, respectively. The large grains have the composition very close to the nominal one. But an obvious scattering in composition was observed in the fine grains. The reason for generating such bimodal microstructure is not totally clear, but it is highly possible due to the different phase relationship at the low temperature during heating up from that at the sintering temperature at 1600 ^{o}C, making it difficult to achieve homogeneity in composition and also microstructure [19-21].

3.3 Proton concentration

Proton concentration calculated from the water content determined by Karl-Fischer titration method is shown in **Fig. 6**. For each sample, the proton concentration decreased with the hydration temperature increased from 300 to 600 ^{o}C. And the protons concentration shows an increasing tendency with the increasing dopant contents, since the oxide ion vacancies ($V_O^{\cdot\cdot}$) essential for the hydration reaction (Eq. 1) to introduce protons ($OH_O^{\cdot}$) is increased by increasing the dopant content ($M_{Zr}^{\prime}$), as shown Eq. 2.

$$H_2O + V_O^{\cdot\cdot} = 2OH_O^{\cdot} \quad [1]$$

$$M_2O_3 + Zr_{Zr}^{\times} + O_O^{\times} \rightarrow M'_{Zr} + ZrO_2 + V_O^{\cdot\cdot} \quad [2]$$

3.4 Bulk and Grain Boundary Conductivity

Electrochemical impedance spectra were measured, and the representative spectra at 110, 300 and 600 ^{o}C in wet H_2 atmosphere are shown in **Fig. 7**. Contributions from bulk, grain boundary conductions, and the electrode reaction are separated on the basis of difference in their specific capacitance around 10^{-11}, 10^{-9}, and 10^{-6} F, respectively. [22] The bulk and grain boundary conductivities are calculated following Eq. 3, in which σ is the conductivity, R is the resistance belonging to bulk or grain boundary fitted from the impedance spectra. L and S are the thickness and surface area of the pellet-like sample for measurement, respectively. The bulk and grain boundary conductivities thereby determined are plotted in **Fig. 8** and **Fig. 9**, respectively, with the data of $BaZr_{0.8}Y_{0.2}O_{3-\delta}$ as reference. Regardless of which dopant was introduced, the bulk conductivity with the dopant content of 0.02 and 0.05 are obviously lower than those with a higher dopant content. Although difference in the bulk conductivity still exists, but such difference is comparably weakened between the samples with the dopant content varying from 0.15 to 0.3, as shown in **Fig. 8**.

$$\sigma = \frac{L}{R \times S} \quad [3]$$

Referring to the grain boundary conductivity, as shown in **Fig. 9**, it increases with the dopant content increasing from 0.02 to 0.2. Although for the Tm-doped samples, the grain boundary conductivity of $BaZr_{0.75}Tm_{0.25}O_{3-\delta}$ is a little higher than that of $BaZr_{0.8}Tm_{0.2}O_{3-\delta}$ (**Fig. 9(c)**), in most cases, further

increasing the dopant content from 0.2 to 0.25 and 0.3 does not help in improving the grain boundary conduction.

3.5 Activation Energy and Pre-exponential Factor of Bulk Conduction

Fig. 10 shows activation energy (E_a) and pre-exponential factor (A) of the bulk conduction in wet H_2 atmosphere extracted by fitting the conductivity data collected between 100 and 250 °C following Eq. 4, in which T is temperature, and k_B is Boltzmann's constant. In general, regardless of which dopant was introduced, both the activation energy and the pre-exponential factor of the bulk conduction have the tendency to increase with the increasing dopant content. And when the dopant content is between 0.02 and 0.2, the value of the activation energy and pre-exponential factor are with the general sequence of Ho, Er > Yb > Tm. When the dopant content increased to 0.25 and 0.3, such general sequence changed to be Tm > Ho, Er > Yb. The values of the activation energy and pre-exponential factor are listed in **Table 1**.

$$\sigma T = A \exp(\frac{-E_a}{k_B T}) \quad [4]$$

3.6 Total Conductivity

Concern with the aim for practical application should be placed on the total conductivity. As shown in **Fig. 11**, the total conductivity increased when the content of Ho, Er, Tm or Yb increased from 0.02 to 0.2. Expect for the case for doping of Tm that the total conductivity of $BaZr_{0.75}Tm_{0.25}O_{3-\delta}$ is close to that of $BaZr_{0.8}Tm_{0.2}O_{3-\delta}$ (**Fig. 11(c)**), further increasing the content of Ho, Er or Yb from 0.2 to 0.25

or 0.3 results in a decrease in the total conductivity. And compared with the value of $BaZr_{0.8}Y_{0.2}O_{3-\delta}$, although there is some difference, strictly speaking, the total conductivities of $BaZr_{0.8}M_{0.2}O_{3-\delta}$ (M = Ho, Er, Tm and Yb) are of the same order with that of $BaZr_{0.8}Y_{0.2}O_{3-\delta}$.

Then, the value at 400, 500 and 600 ^{o}C is plotted in **Fig. 12**. It is quite meaningful to figure out that the total conductivities of $BaZr_{0.8}M_{0.2}O_{3-\delta}$ (M = Ho, Er, Tm and Yb) and $BaZr_{0.75}Tm_{0.25}O_{3-\delta}$ collected at 600 ^{o}C are higher than 0.01 Scm^{-1}, a criteria regarded to be necessary for the application as an electrolyte in fuel cells [23]. Especially, even at 500 ^{o}C, $BaZr_{0.8}Ho_{0.2}O_{3-\delta}$, $BaZr_{0.8}Er_{0.2}O_{3-\delta}$, $BaZr_{0.8}Tm_{0.2}O_{3-\delta}$ and $BaZr_{0.75}Tm_{0.25}O_{3-\delta}$ have the total conductivity satisfying such criteria.

4 Discussion

A model of proton trapping is recently well received on explaining the proton conduction behavior in $BaZrO_3$ [11, 24], which can be briefly summarized as that protons are trapped at the oxide ions near the dopants, but migrate relatively freely at the oxide ions adjacent to the host Zr cations. In order to activate the "trapped" protons to migrate, an association energy has to be conquered. And the dopant with low association energy with protons is suggested by Yamazaki, *et al*. [11] to be a key criterion on choosing a proper dopant for $BaZrO_3$. According to **Fig. 10(a)**, when the dopant content is between 0.02 and 0.2, the activation energy of the bulk conduction in wet hydrogen atmosphere are of a general sequence as Ho, Er > Yb > Tm. Since the activation energy is regarded to be a sum of the migration energy and association energy at low temperature approximation [11], if assuming the migration

energy to be constant, it comes to the conclusion that Tm imparts $BaZrO_3$ with a relatively small association energy, whereas Ho and Er have relatively large association energies with protons. However, when the dopant content increased to higher value such as 0.25 and 0.3, the activation energy in the system containing Tm turns to be higher than that with Ho or Er. Although it is not quite clear, higher dopant content possibly introduce other complicated association between dopants and protons, making the case different from that with relatively low dopant content.

As shown in **Fig. 10(b)**, the pre-exponential factor increased with the increasing dopant content, for which an increase in the concentration of charge carriers (protons) is one of the reasons (**Fig. 6**). In addition, a dependence of pre-exponential factor on the dopants for $BaZrO_3$ is also quite clear in **Fig. 10(b)**. And with the dopant content varying between 0.02 and 0.2, the pre-exponential factor of the Tm-doped samples is smaller than those of the others.

From **Fig. 11**, it can be said that Ho, Er, Tm and Yb also impart $BaZrO_3$ with high total conductivity with the same order as the Y-doped one. Such conclusion no doubt offers a flexible choice on the doping strategy for proton conductive $BaZrO_3$. However, though this work, we still cannot answer the question to what is the best dopant for $BaZrO_3$, since other important factors, such as tolerance against carbon dioxide, transport number of different charge carriers (holes, oxide ions, and protons), are also very important. Our next work will report a study on the transport properties of $BaZrO_3$ doped with different dopants.

5 Conclusions

In this work, a systematic investigation was performed on $BaZrO_3$ doped with various content of Ho, Er, Tm and Yb. It was found that, with the dopant content varying from 0.02 and 0.3, all the samples exhibit a single perovskite phase. In general, the dependence of microstructure on the dopant content behaves in a similar way, regardless of which dopant was introduced. A bimodal microstructure was observed with the dopant content vary from 0.05 to 0.15. $BaZr_{0.85}Tm_{0.15}O_{3-\delta}$ was taken for example to analysis by STEM-EDS point analysis, and it was found that such bimodal microstructure was composed of large grains with homogeneous composition, and fine grains with discrepancy in composition. Then, the electrochemical conductivity was measured, and with the dopant content between 0.02 and 0.2, the samples doped with Tm was found to have the lowest activation energy for bulk conduction in wet H_2. Such result indicates that Tm possibly imparts $BaZrO_3$ with relatively low association energy for proton trapping. And referring to the total conductivity, comparably high value, close to that of $BaZr_{0.8}Y_{0.2}O_{3-\delta}$, was obtained for the samples of $BaZr_{0.8}Ho_{0.2}O_{3-\delta}$, $BaZr_{0.8}Er_{0.2}O_{3-\delta}$, $BaZr_{0.8}Tm_{0.2}O_{3-\delta}$, $BaZr_{0.8}Yb_{0.2}O_{3-\delta}$ and $BaZr_{0.75}Tm_{0.25}O_{3-\delta}$.

Acknowledgement

This study was supported by the New Energy and Industrial Technology Development Organization (NEDO) in Japan (project code P08023). The authors also want to thank Dr. Masatoshi Majima at Sumitomo Electric Industries, Ltd., for valuable discussion, and Mr. Kenji Kazumi for STEM-EDS analysis.

References

1. H. Iwahara, T. Esaka, H. Uchida, and N. Maeda, *Solid State Ionics*, **3-4**, 359 (1981).

2. H. Iwahara, H. Uchida, and S. Tanaka, *Solid State Ion*ics, **9-10**, 1021 (1983).

3. W.G. Coors, *J. Power Sources*, **118**, 150 (2003).

4. Y. Guo, Y. Lin, R. Ran, and Z. Shao, *J. Power Source*, **193**, 400 (2009).

5. L. Yang, S. Wang, K. Blinn, M. Liu, Z. Liu, and M. Liu, *Science*, **326**, 126 (2009).

6. Y. Okumura, Y. Nose, J. Katayama, and T. Uda, *J. Electrochem. Soc*., **158**, B1067 (2011).

7. C. Duan, J. Tong, M. Shang, S. Nikodemski, M. Sanders, S. Ricote, A. Almansoori, and R. O'Hayre, *Science*, **349**, 1321 (2015).

8. L. Bi, S.P. Shafi, and E. Traversa, *J. Mater. Chem. A*, **3**, 5815 (2015).

9. T. Norby, M. Widerøe, R. Glöckner, and Y. Larring, *Dalton Trans*., **19**, 3012 (2004).

10. D. Pergolesi, E. Fabbri, A. D'Epifanio, E.D. Bartolomeo, A. Tebano, S. Sanna, S. Licoccia, G. Balestrino, and E. Traversa, *Nat. Mater*., **9**, 846 (2010).

11. Y. Yamazaki, F. Blanc, Y. Okuyama, L. Buannic, J.C. Lucio-Vega, C.P. Grey, and S.M. Haile, *Nature Mater*., **12**, 647 (2013).

12. S. Imashuku, T. Uda, Y. Nose, G. Taniguchi, Y. Ito, and Y. Awakura, *J. Electrochem. Soc.*, **156**, B1 (2009).

13. D. Han, Y. Nose, K. Shinoda, and T. Uda, *Solid State Ionics*, **213**, 2 (2012).

14. D. Han, K. Shinoda, S. Sato, M. Majima, and T. Uda, *J. Mater. Chem. A*, **3**, 1243 (2015).

15. D. Han, Y. Okumura, Y. Nose, and T. Uda, *Solid State Ionics*, **181**, 1601 (2010).

16. D. Han, K. Kishida, K. Shinoda, H. Inui, and T. Uda, *J. Mater. Chem. A*, **1**, 3027 (2013).

17. D. Han, K. Shinoda, and T. Uda, *J. Am. Ceram. Soc*., **97**, 643 (2014).

18. R.D. Shannon, *Acta Crystallogr. Sect. A*, **32**, 751 (1976).

19. S. Imashuku, T. Uda, Y. Nose, and Y. Awakura, *J. Phase Equilib. Diff.*, **31**, 348 (2010).

20. S. Imashuku, T. Uda, Y. Nose, and Y. Awakura, *J. Alloys Compd*., **509**, 3872 (2011).

21. D. Han, N. Hatada, and T. Uda, submitted to *J. Am. Ceram. Soc.*

22. S.M. Haile, D.L. West, and J. Campbell, *J. Mater. Res*., **13**, 1576 (1998).

23. B.C.H. Steele, and A. Heinzel, *Nature*, **414**, 345 (2001).

24. F. Blanc, L. Sperrin, D. Lee, R. Dervisoğlu, Y. Yamazaki, S.M. Haile, G. De Paëpe, and C.P. Grey, *J. Phy. Chem. Lett*., **5**, 2431 (2014).

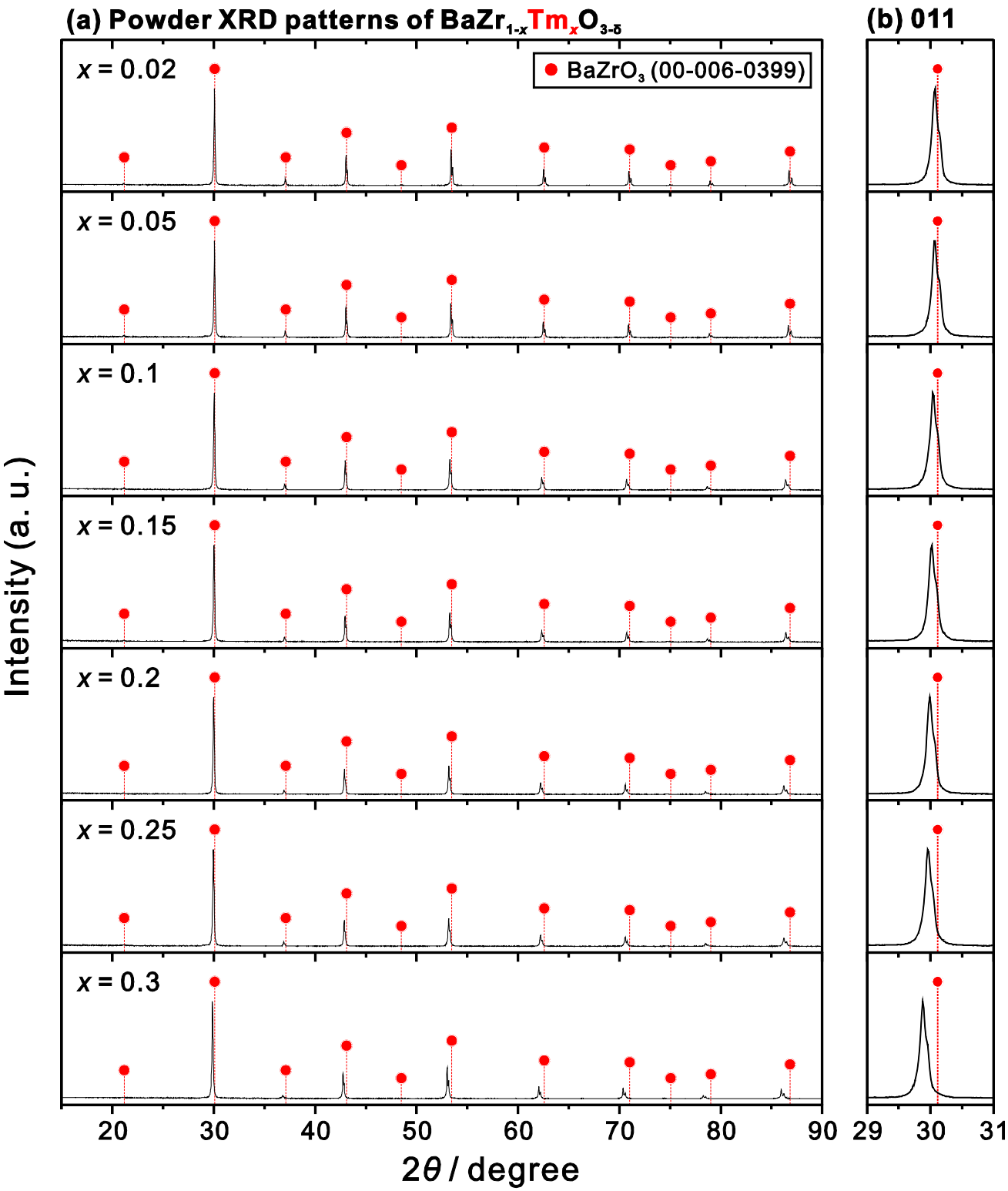

Fig. 1 (a) Powder XRD patterns of $BaZr_{1-x}Tm_xO_{3-\delta}$ (x = 0.02, 0.05, 0.1, 0.15, 0.2, 0.25 and 0.3), with the 011 diffraction peak emphasized in (b) to show a clear peak shift with the Tm content. All the samples were sintered at 1600 ^{o}C in O_2 for 24 h.

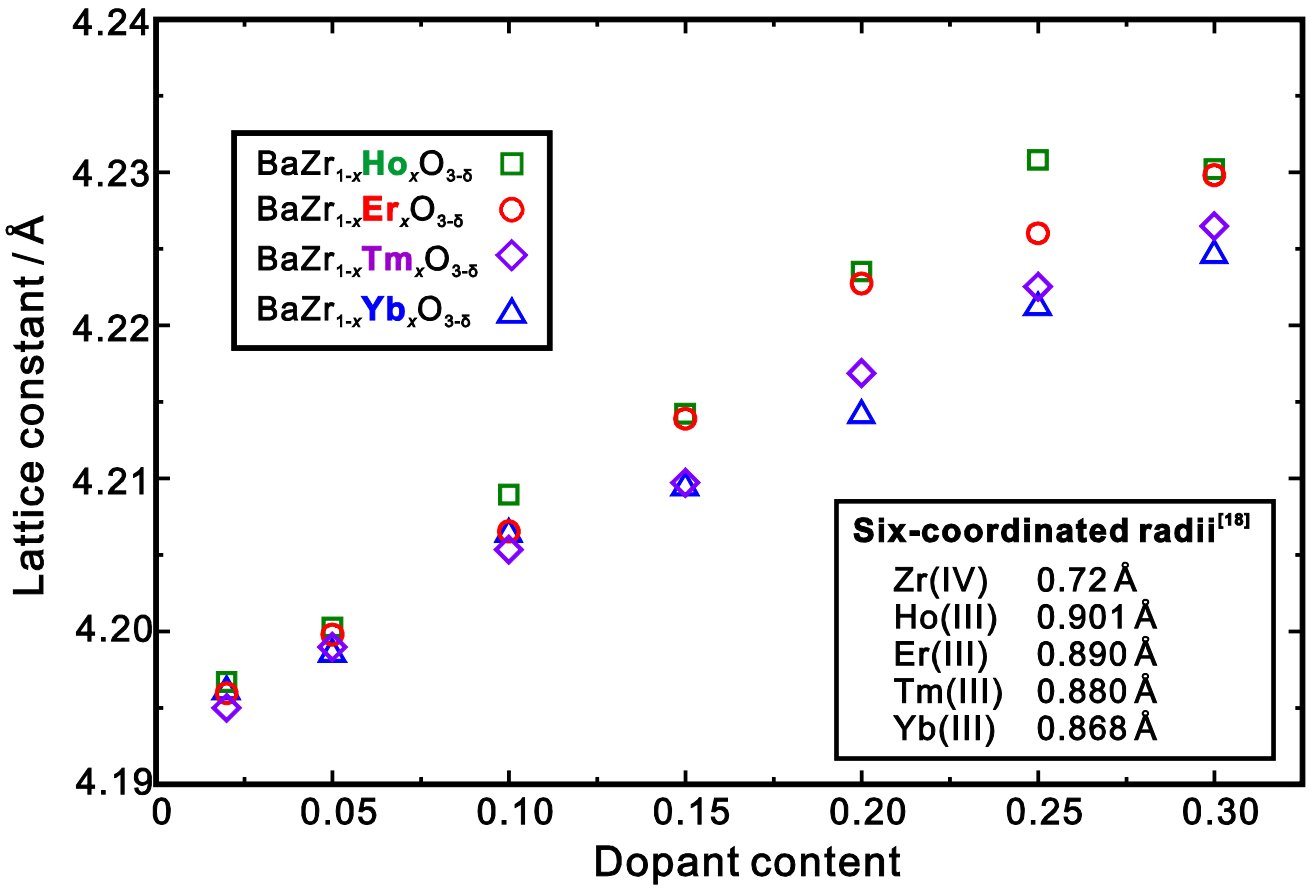

Fig. 2 Lattice constants of $BaZr_{1-x}M_xO_{3-\delta}$ (M = Ho, Er, Tm and Yb, x = 0.02, 0.05, 0.1, 0.15, 0.2, 0.25 and 0.3). The lattice constants were calculated by simulate the powder XRD patterns of the samples sintered at 1600 ^{o}C in O_2 for 24 h with Rietveld refinement.

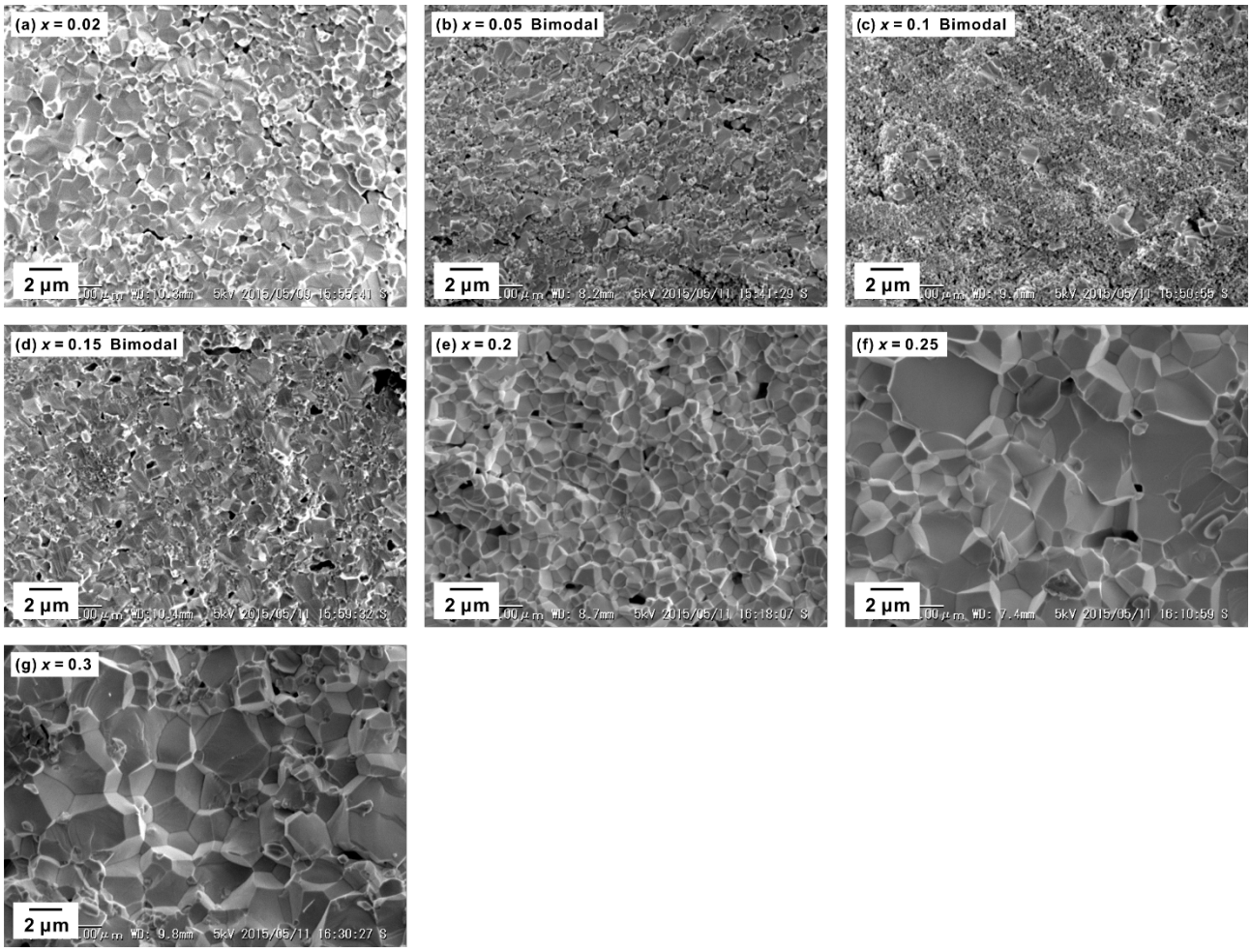

Fig. 3 SEM image of the fractured cross-section of the samples of $BaZr_{1-x}Tm_xO_{3-\delta}$ (x = 0.02, 0.05, 0.1, 0.15, 0.2, 0.25 and 0.3). All the samples were heat-treated at 1600 ^oC in O_2 for 24 h for sintering.

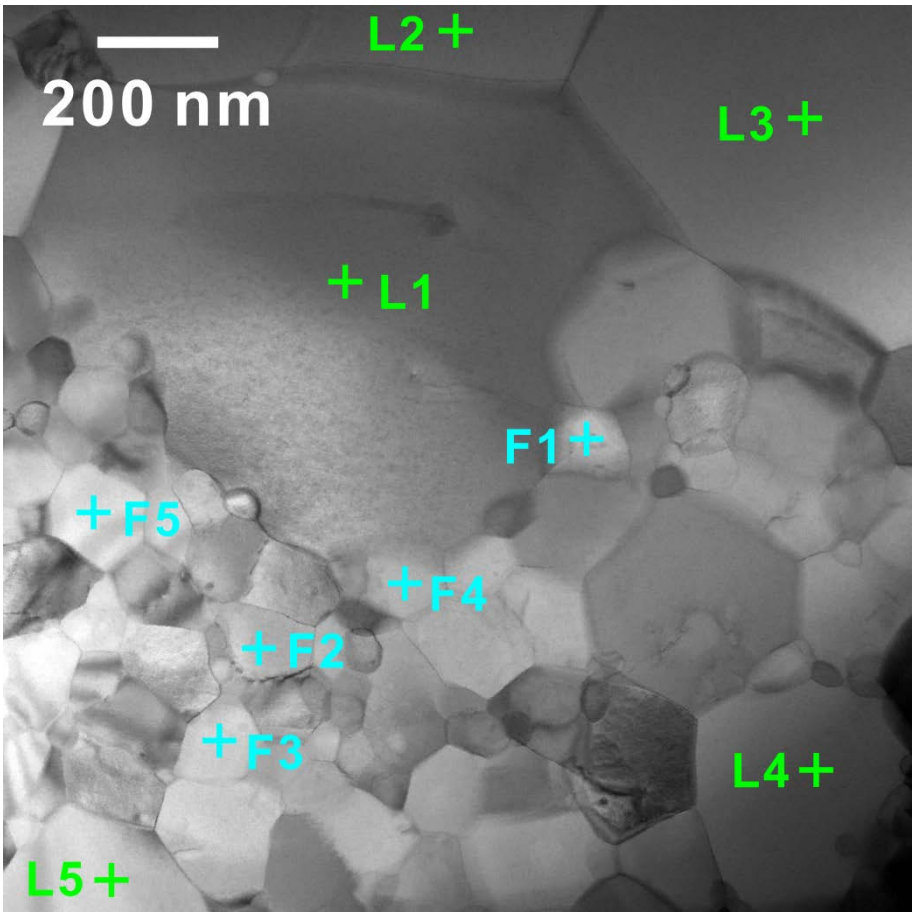

Fig. 4 A bright field STEM (BF-STEM) image of $BaZr_{0.85}Tm_{0.15}O_{3-\delta}$ (BZTm15) clearly showing a bimodal microstructure composed of large grains (L1 to L5) and fine grains (F1 to F5). The sample was heat-treated at 1600 ^{o}C in O_2 for 24 h for sintering. The results of STEM-EDS point analysis of L1 to L5 and F1 to F5 are given in **Table 1**.

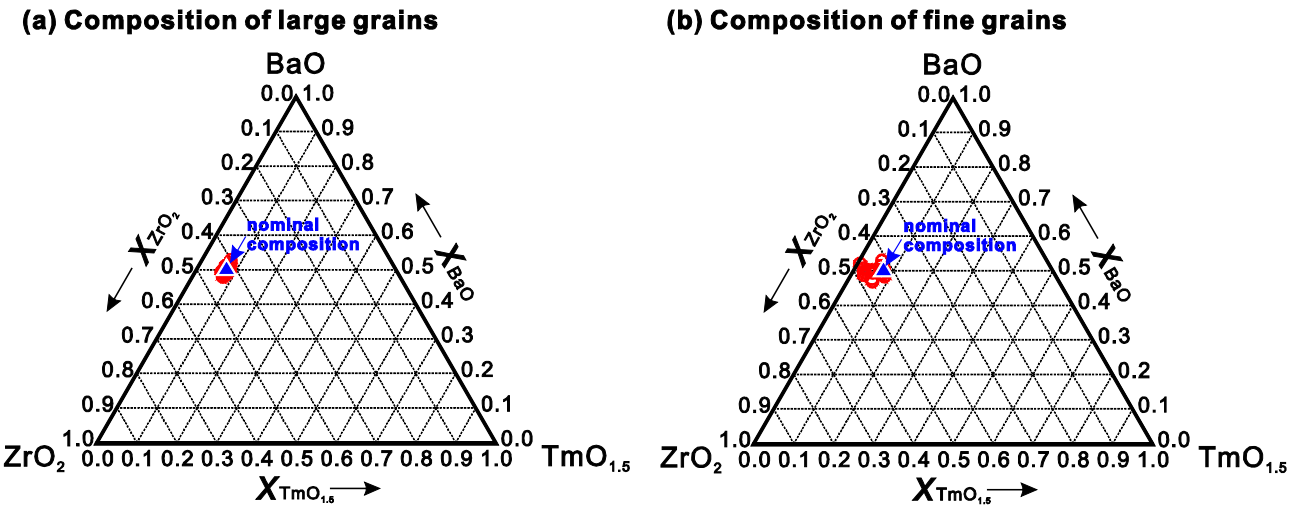

Fig. 5 Compositions of the (a) large grains, and (b) fine grains of $BaZr_{0.85}Tm_{0.15}O_{3-\delta}$ (BZTm15) determined by STEM-EDS point analysis. The sample was heat-treated at 1600 ^{o}C in O_2 for 24 h for sintering.

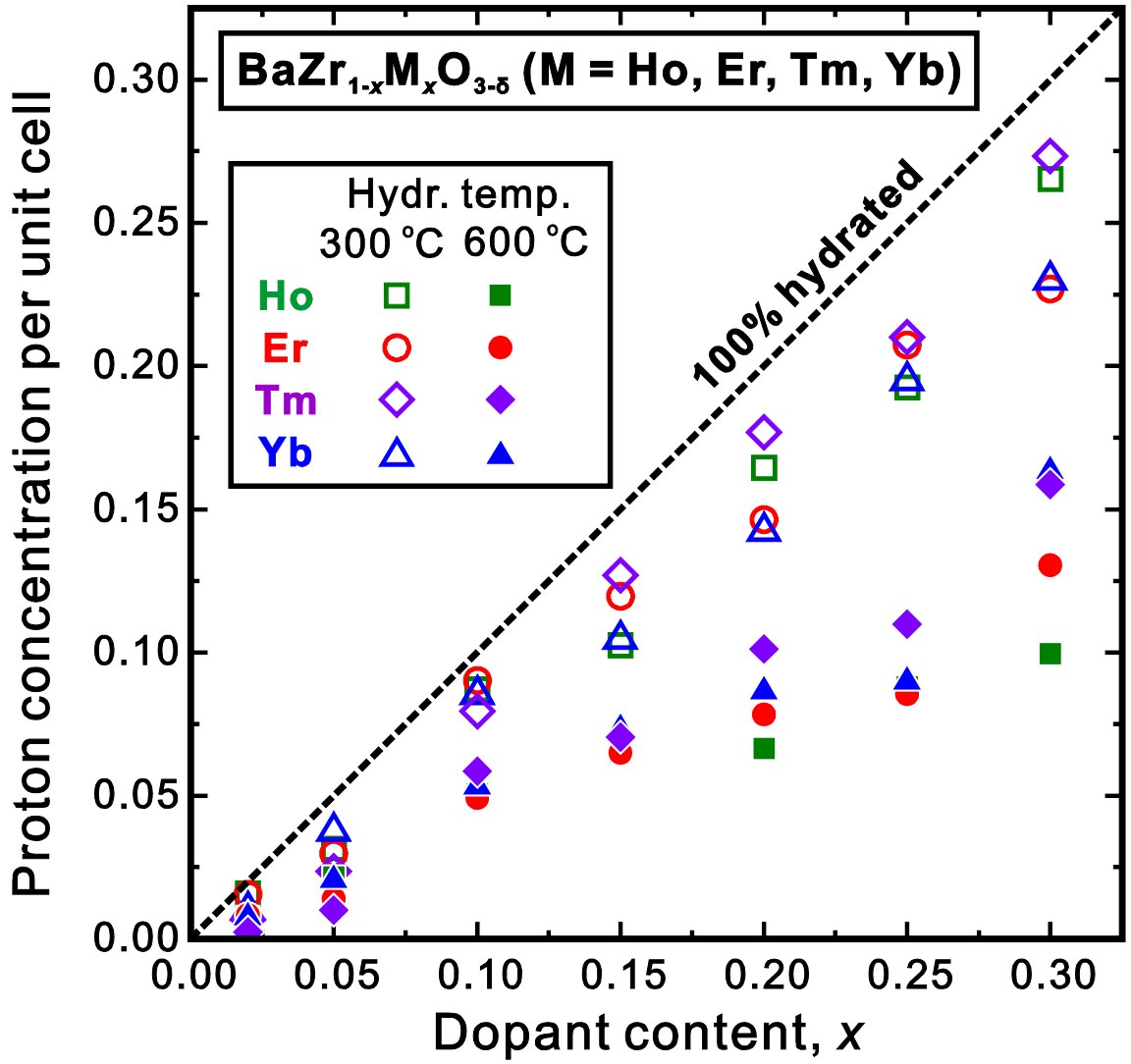

Fig. 6 Proton concentration of the samples of $BaZr_{1-x}M_xO_{3-\delta}$ (M = Ho, Er, Tm and Yb, x = 0.02, 0.05, 0.1, 0.15, 0.2, 0.25 and 0.3). All the samples were sintered at 1600 °C in O_2 for 24 h, and hydrated at 300 or 600 °C in wet Ar (p_{H_2O} = 0.05 atm). The proton concentration was calculated from the water content measured by Karl-Fischer titration method.

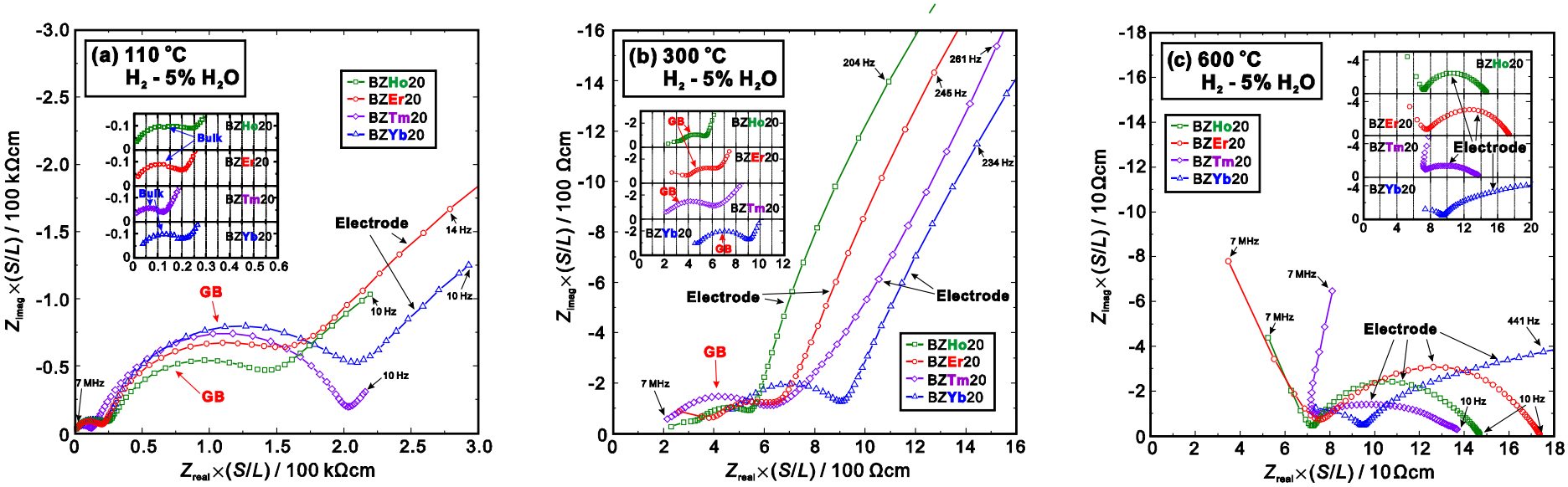

Fig. 7 Representative electrochemical impedances spectra of $BaZr_{0.8}M_{0.2}O_{3-\delta}$ (BZM20, M = Ho, Er, Tm, Yb) collected at (a) 110 °C, (b) 300 °C, and (c) 600 °C to give examples of separation of semicircles belonging to contributions from bulk and grain boundary conductions, which were identified from their specific capacitances with the order of 10^{-11} and 10^{-9} F, respectively. Magnified views of the semicircles belonging to the bulk conduction at 110 °C, and those belonging to grain boundary conduction and electrode reaction at 300 and 600 °C are given in insets.

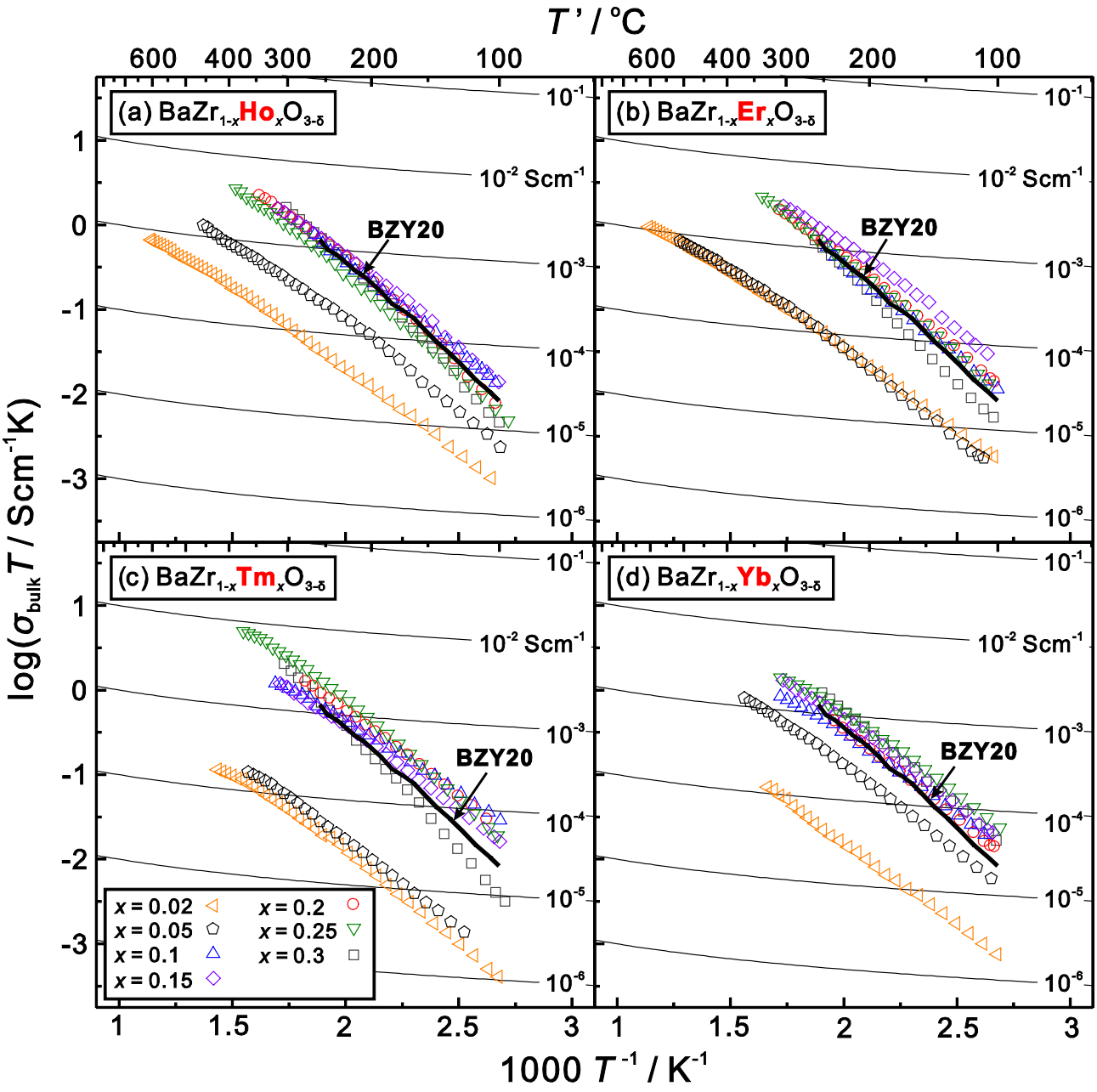

Fig. 8 Arrhenius plots of bulk conductivity of $BaZrO_3$ doped with various content of (a) Ho, (b) Er, (c) Tm and (d) Yb in H_2 – 5% H_2O atmosphere. All the samples were finally heat-treated at 1600 °C in O_2 for 24 h. The bulk conductivity of $BaZr_{0.8}Y_{0.2}O_{3-\delta}$ in wet H_2 are also plotted as reference.

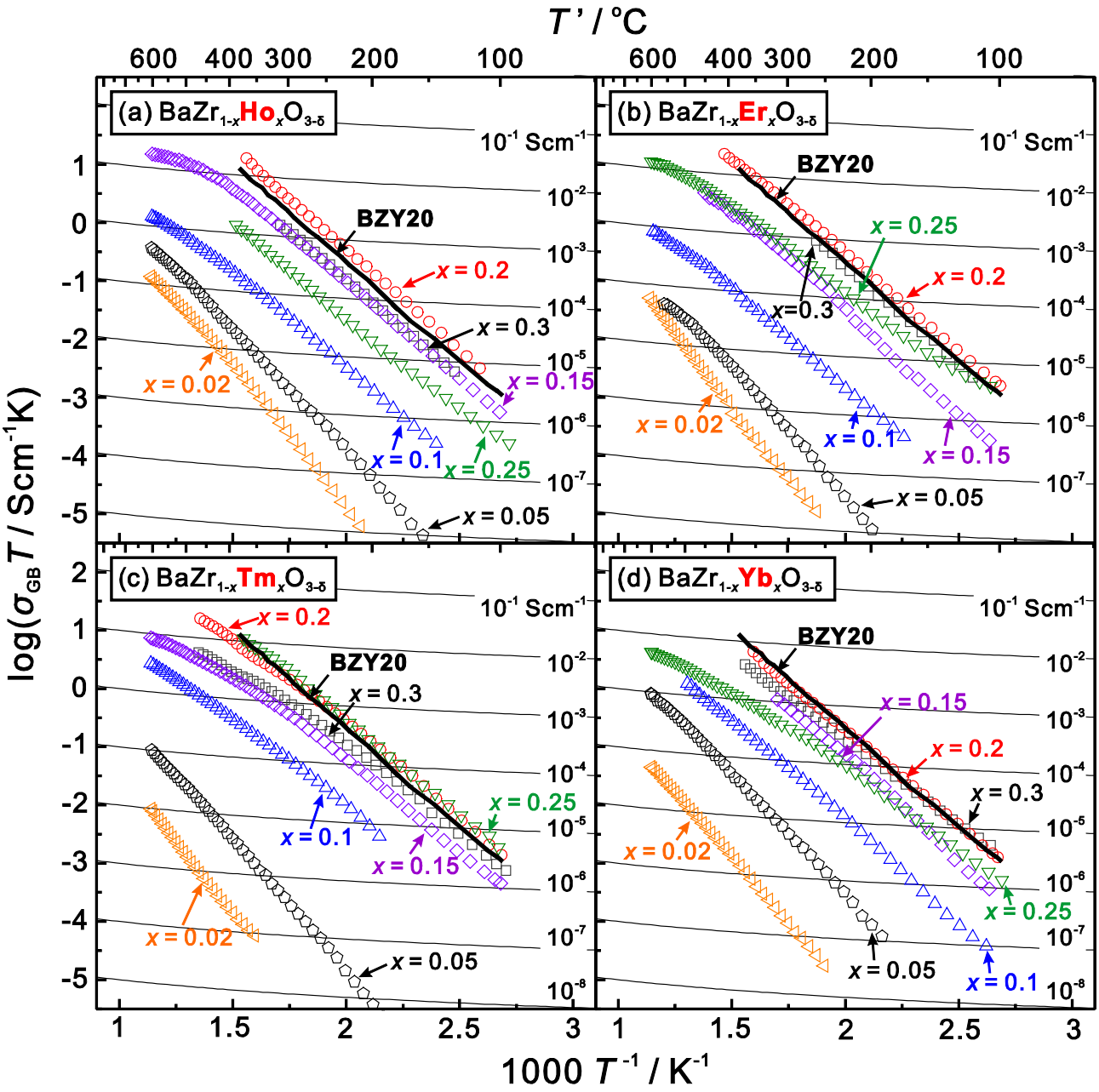

Fig. 9 Arrhenius plots of grain boundary conductivity of $BaZrO_3$ doped with various content of (a) Ho, (b) Er, (c) Tm and (d) Yb in H_2 – 5% H_2O atmosphere. All the samples were finally heat-treated at 1600 °C in O_2 for 24 h. The grain boundary conductivity of $BaZr_{0.8}Y_{0.2}O_{3-\delta}$ in wet H_2 are also plotted as reference.

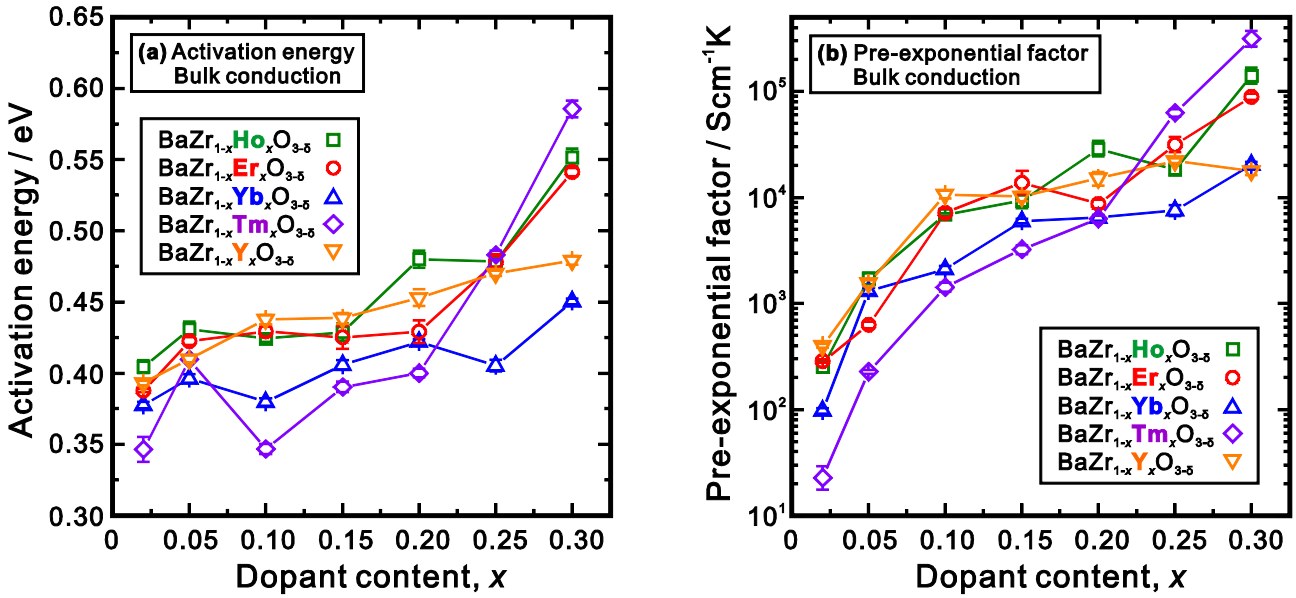

Fig. 10 (a) Activation energy, and (b) pre-exponential factor of the bulk conduction of $BaZr_{1-x}M_xO_{3-\delta}$ (M = Ho, Er, Yb and Tm, x = 0.02, 0.05, 0.1, 0.15, 0.2, 0.25 and 0.3) in H_2 – 5% H_2O atmosphere. The values for Y-doped samples [21] are plotted for comparison.

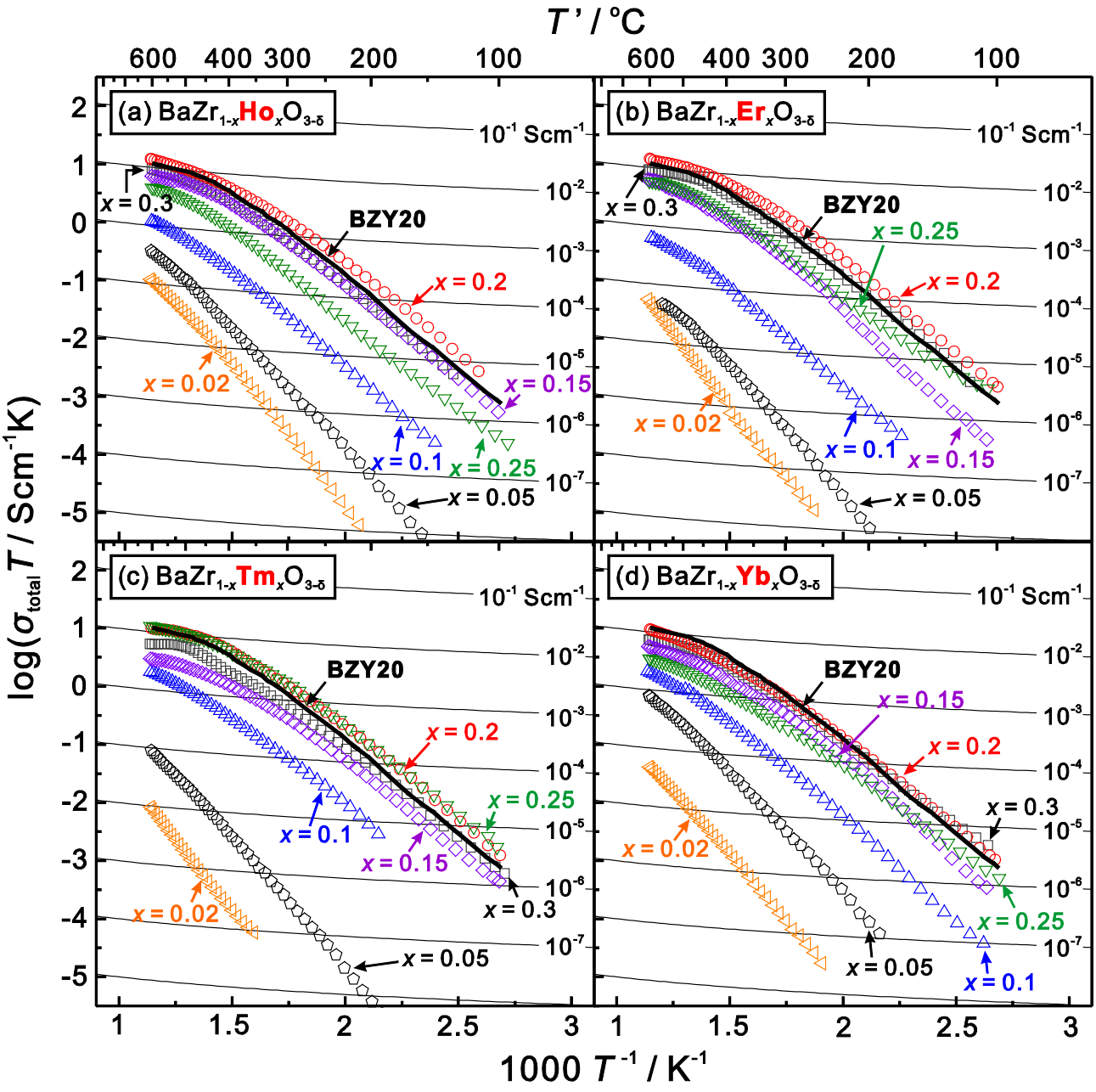

Fig. 11 Arrhenius plots of total conductivity of $BaZrO_3$ doped with various content of (a) Ho, (b) Er, (c) Tm and (d) Yb in H_2 – 5% H_2O atmosphere. All the samples were finally heat-treated at 1600 °C in O_2 for 24 h. The total conductivity of $BaZr_{0.8}Y_{0.2}O_{3-\delta}$ in wet H_2 are also plotted as reference.

Table 1 Activation energy and pre-exponential factors of bulk conduction of $BaZrO_3$ doped with various Ho, Er, Tm and Yb in H_2 – 5% H_2O by fitting the conductivity collected in the temperature of 100 – 250 °C. The data for the samples with 20 mol% dopant is cited from our previous work [14].

	Dopants for Zr site							
	Ho		Er		Yb		Tm	
Dopant content	Activation energy / eV	Pre-exponential factor / $Scm^{-1}K$	Activation energy / eV	Pre-exponential factor / $Scm^{-1}K$	Activation energy / eV	Pre-exponential factor / $Scm^{-1}K$	Activation energy / eV	Pre-exponential factor / $Scm^{-1}K$
0.02	0.405(4)	$2.54(31) \times 10^2$	0.388(1)	$2.86(10) \times 10^2$	0.377(2)	$9.71(55) \times 10^1$	0.346(9)	$2.26(52) \times 10^1$
0.05	0.431(5)	$1.72(23) \times 10^3$	0.423(3)	$6.29(44) \times 10^2$	0.396(3)	$1.31(9) \times 10^3$	0.410(2)	$2.28(10) \times 10^2$
0.1	0.424(2)	$6.93(18) \times 10^3$	0.429(3)	$7.19(66) \times 10^3$	0.380(3)	$2.11(15) \times 10^3$	0.347(4)	$1.42(15) \times 10^3$
0.15	0.429(6)	$9.35(150) \times 10^3$	0.425(8)	$1.38(30) \times 10^4$	0.406(3)	$5.99(31) \times 10^3$	0.390(4)	$3.23(31) \times 10^3$
0.2	0.480(6)	$2.88(44) \times 10^4$	0.429(4)	$8.74(81) \times 10^3$	0.422(2)	$6.45(40) \times 10^3$	0.400(3)	$6.32(45) \times 10^3$
0.25	0.478(4)	$1.83(18) \times 10^4$	0.478(5)	$3.16(48) \times 10^4$	0.405(4)	$7.57(86) \times 10^3$	0.483(3)	$6.28(50) \times 10^4$
0.3	0.551(6)	$1.40(23) \times 10^5$	0.541(3)	$8.90(63) \times 10^4$	0.450(2)	$2.04(12) \times 10^4$	0.586(6)	$3.13(49) \times 10^5$